CLOSURE LAW MODEL UNCERTAINTY QUANTIFICATION

Andreas Strand,[1,*] Jørn Kjølaas,[2] Trond H Bergstrøm,[2] Ingelin Steinsland,[3] & Leif Rune Hellevik[1]

[1]*Department of Structural Engineering, Faculty of Engineering, Norwegian University of Science and Technology, 7491 Trondheim, Norway*

[2]*Department of Process Technology, SINTEF Industry, 7465, Trondheim, Norway*

[3]*Department of Mathematical Sciences, Faculty of Information Technology and Electrical Engineering, Norwegian University of Science and Technology, 7491 Trondheim, Norway*

*Address all correspondence to: Andreas Strand, E-mail: andreas.strand@ntnu.no

Original Manuscript Submitted: 01/15/2021; Final Draft Received: mm/dd/yyyy

The prediction uncertainty in simulators for industrial processes is due to uncertainties in the input variables and uncertainties in specification of the models, in particular the closure laws. In this work, the uncertainty in each closure law was modeled as a random variable and the parameters of its distribution were optimized to correctly quantify the uncertainty in predictions. We have developed two methods for optimization, based on the integrated quadratic distance and the energy score.

The proposed methods were applied to the commercial multiphase flow simulator LedaFlow with the liquid volume fraction and pressure gradient as output variables. Two datasets were analyzed. Both describe two-phase gas-liquid flow, but are otherwise fundamentally different. One is gas-dominated stratified/annular flow and the other is liquid-dominated slug flow. The closure law for the gas-wall friction factor is decisive for the gas-dominated predictions, and the estimated relative standard deviation is 4.5 % *or* 8.0 % *depending on method. The liquid-dominated study showed that the liquid-wall friction factor and the slug bubble velocity are the closure laws with the greatest impact. Moreover, the estimated relative standard deviation in the liquid-wall friction factor is* 5 %*, and the deviation in the slug bubble velocity is* 4 %*. We used direct measurements of the slug bubble velocity to validate the estimated uncertainty.*

KEY WORDS: *multiphase flow, ledaflow, closure laws, uncertainty propagation, prediction*

1. INTRODUCTION

Closure laws are approximate relationships used to remove unknowns from a model. They appear in most sciences. In electrical circuits Ohm's law is used to relate voltage and current as part of a larger network analysis [1]. It is an empirical law which can also be derived by applying classical mechanics to electrons in a microscopic model [2]. In fact, many closure laws are macroscopic averages of simplified microscopic models which are additionally supported by experiments. Another example is the ideal gas law which is used in thermodynamic processes [3]. It was discovered by experiments, but can be derived from kinetic theory. The ideal gas law is most accurate for gases of small molecules at high temperature and low pressure. Similarly, Ohm's law is most accurate for ohmic materials like metals. Another example is Darcy's law for flow through a porous medium [4], where the pressure gradient is proportional to flux, but where a quadratic term is required for large Reynolds numbers [5]. Closure laws can still be useful when the assumptions are slightly violated. To quantify the uncertainty of predictions when assumptions are violated, we need to be able to quantify how much the truth deviates from the closure law. When the closure laws are part of a larger model, the effect of the deviations in prediction can be modeled with uncertainty propagation. More examples of closure laws are described in Section 3.1 when introducing case studies.

2152–5080/21/$35.00

We considered two case studies of pipe flow with oil, water and gas combined. This is an example of *multiphase flow* because the flow is simultaneous in two thermodynamic phases [6]. Multiphase flow occurs in both nature and industry. In rain, sea waves and sedimentation, water interacts with air or particles. Blood flow is a mixture of plasma, red blood cells and more. Industry examples are cooling systems for nuclear reactors and the exhaust of cars.

Multiphase flow simulators are essential for design and operation of pipelines for petroleum transport. The majority of commercial software is based on simplified zero- or one-dimensional physical descriptions and are tuned to large amounts of data. Prediction errors are inevitable, and describing them is imperative. The prediction errors can be described using an uncertainty framework combining uncertainty in input and model.

In 1988, the Nuclear Regulatory Commission deployed the Code Scaling, Applicability, and Uncertainty evaluation methodology for emergency core cooling systems of power plants [7], which was demonstrated on a large break loss of coolant accident in a pressurized water reactor and published as a collection of papers [8–12]. They produced a *phenomena identification and ranking table* [8,13] according to the expected effect on the response variable *peak clad temperature*. Further screening from analytical sensitivity calculations [14] yielded a set of 28 inputs/parameters [9]. The uncertainty distributions for each variable was determined from an extensive collection of laboratory experiments, literature and was compared to operating plant experience. After another sensitivity study, 7 variables were selected for uncertainty propagation. They used regression to make a surrogate model for the simulator, and produced $95\,\%$ lower confidence intervals for peak clad temperature.

Cremaschi et al. [15] explained the need for incorporating uncertainty into multiphase simulators. Specifically, they made a call for researchers to accompany each input measurement with an uncertainty estimate to be propagated through the simulator. The result is prediction uncertainty partitioned into contributions from each input through its measurement uncertainty. However, model uncertainty was not discussed. Forward propagation of uncertainty through two-phase models with Monte Carlo methods and polynomial chaos expansions have been applied [16,17].

Holm et al. [18,19] consider both input and model uncertainty for the multiphase simulator OLGA applied to the Shtokman oil and gas field. The simulator uses several closure laws and the authors change the output from each closure law by $\pm\,30\,\%$ and measure how sensitive the model predictions are. They suggest that the impact of each closure law depends on the flow regime, which indeed is confirmed in a later study with laboratory experiments [20]. The value of $30\,\%$ error is an estimate based on experience, but it is potentially conservative.

There are several studies of closure law uncertainty in single-phase flow in the 2010s. A frequent example is the Reynolds-averaged Navier-Stokes equation, where a Reynolds stress model describes turbulent fluctuations. The uncertainty in the Reynolds stress model have been estimated through different models based on prior knowledge and whether data is available [21,22]. It is also possible to build a rigorous framework incorporating input and model uncertainty using probability logic and Bayes' theorem [23,24]. The simulator is then described as a dynamic model with unknown parameters. Data is used as evidence to estimate the parameters and the posterior distribution. In principle, this approach is general and could also serve multiphase flow.

We have developed two accessible data-driven methods for estimating closure law uncertainty which in combination with input uncertainty yield predictions with realistic uncertainty. The methods were applied to the simulator LedaFlow using two recent experiment series with different flow conditions. Additionally, we validated the methods using direct closure law measurements. The framework and methods are presented in section 2, and two case studies are demonstrated in section 3. In section 4 the methods and results are discussed, followed by conclusions.

2. METHODS

2.1 Probabilistic simulator with uncertainty in closure laws

We here describe how to construct a simulator incorporating uncertainty in both model and measurements of input variables. Note that throughout the text, hat accent denotes estimates, bold letters are vectors or matrices and capital letters are random variables. The random variables have inherent uncertainty and are used in place of unknown exact values. For instance, measured variables are represented by random variables because of their inherent measurement uncertainty.

Simulators apply a set of governing equations such as differential equations and algebraic expressions, including

Nomenclature

$\circ$	function composition
c	number of closure laws
$\mathrm{d}^r\boldsymbol{\delta}$	r-dimensional volume differential
$\mathrm{E}\|\|\cdot\|\|_1$	expected value of the ℓ_1 norm
es_i	energy score for experiment i
ES	average energy score
f	true model
$\hat{f}$	probabilistic simulator
$\hat{f}^{\mathrm{o}}$	deterministic simulator
$\hat{F}$	empirical distribution of observed errors
$\hat{F}^{\mathrm{s}}$	empirical distribution of sampled errors
g_k	true closure law
$\hat{g}_k$	simulator closure law
G_k	probabilistic closure law
i	index for experiment
I	indicator function
IQ	integrated quadratic distance
j or l	index for Monte Carlo sample
k	index for model operation
m	number of Monte Carlo samples for each variable
n	number of experiments
p	number of inputs
r	number of outputs
$\mathbb{R}^r$	r-dimensional real coordinate space
u	state of the physical system
$\mathbf{W}_i$	error weights
$\mathbf{x}_i$	physical value of input
$\mathbf{X}_i$	measured value of input
$\mathbf{Y}_i$	measured value of output
$\hat{\mathbf{Y}}_i^{\mathrm{o}}$	default predictions
$\hat{\mathbf{Y}}_{ij}^{\mathrm{s}}$	sampled predictions

Greek Symbols

Γ_k	sampled error in closure law
$\boldsymbol{\delta}$	argument of empirical distribution function
Δ_i	observed errors
Δ_{ij}^{s}	sampled errors
$\boldsymbol{\varepsilon}_i^{\mathbf{x}}$	measurement error in input
$\boldsymbol{\varepsilon}_{ij}^{\mathbf{x}}$	sampled measurement error in input
$\boldsymbol{\varepsilon}_i^{\mathbf{Y}}$	measurement error in output
$\boldsymbol{\varepsilon}_{ij}^{\mathbf{Y}}$	sampled measurement error in output
$\boldsymbol{\theta}$	parameters of the probabilistic simulator
$\hat{\boldsymbol{\theta}}$	parameter estimates
μ	closure law bias
σ	standard deviation

closure laws $\mathbf{g} = (g_1, g_2, \ldots, g_c)$. The state u of the system is the solution to the set of equations

$$\mathcal{R}\left(u, \mathbf{g}(u); \mathbf{x}\right) = 0, \tag{1}$$

which depends on input variables $\mathbf{x} = (x_1, x_2, \ldots, x_p)$. The quantities of interest, henceforth called output, are functions $q(u)$ of the state u. Because the state depends on input, we can also write the output as $f(\mathbf{x}) = q(u(\mathbf{x}))$. General uncertainty quantification in the framework of (1) and Bayesian inference was discussed by Oliver et al. [25].

The closure laws $\mathbf{g}$, input variables $\mathbf{x}$ and output $f(\mathbf{x})$ are in practice unknown and instead represented by measurements or approximations. For instance, the measured output denoted $\mathbf{Y} = (Y_1, Y_2, \ldots, Y_r)$ may be represented as

$$\mathbf{Y} = f(\mathbf{x}) + \boldsymbol{\varepsilon}^{\mathbf{Y}}, \tag{2}$$

where $\boldsymbol{\varepsilon}^{\mathbf{Y}} = (\varepsilon_1^{\mathbf{Y}}, \varepsilon_2^{\mathbf{Y}}, \ldots, \varepsilon_r^{\mathbf{Y}})$ are random variables representing measurement error for output variables. Furthermore, each g_k in (1) is approximated by curve fitting or assumptions. Approximations $\hat{g}_k(u, \mathbf{x})$ are the closure laws actually implemented in a simulator. Substituting $\hat{\mathbf{g}} = (\hat{g}_1, \hat{g}_2, \ldots, \hat{g}_c)$ for $\mathbf{g}$, changes the solution u. The resulting output function $\hat{f}^{\mathrm{o}}(\mathbf{x})$ will be referred to as the *deterministic simulator* and may represent a commercial software for predicting output. Large model errors in approximating closure laws may cause the deterministic simulator output $\hat{f}^{\mathrm{o}}(\mathbf{x})$ to deviate critically from the correct output $f(\mathbf{x})$.

The main challenge we address is to quantify the model errors. The proposed solution is to introduce random variables $G_k(u, \mathbf{x}, \boldsymbol{\theta})$ as an extension of $\hat{g}_k(u, \mathbf{x})$ with random errors incorporated, where $\boldsymbol{\theta}$ are the distributional parameters of $\mathbf{G}$. The added errors represent epistemic uncertainty about the closure law due to limited knowledge. Substituting $\mathbf{G} = (G_1, G_2, \ldots, G_c)$ for $\mathbf{g}$ in (1) results in the *probabilistic simulator* $\hat{f}(\mathbf{x}; \boldsymbol{\theta})$. One example of a probability model for a closure law is $G_k(u, \mathbf{x}, \boldsymbol{\theta}) = \hat{g}_k(u, \mathbf{x}) + \Gamma_k(\mathbf{x}, \boldsymbol{\theta})$, where $\Gamma_k(\mathbf{x}, \boldsymbol{\theta})$ is a uniform error variable. Generally, the probability model is a qualified estimate for potential misspecification of the closure law and is in general individual to each experiment.

2.2 Simulator predictions

The method described below is driven by experiments $i = 1, 2, \ldots, n$ with measured input $\mathbf{X}_i$ and measured output $\mathbf{Y}_i$. The measured input is different from the physical value $\mathbf{x}_i$ and we assume that the difference $\boldsymbol{\varepsilon}_i^{\mathbf{x}} = \mathbf{X}_i - \mathbf{x}_i$ is measurement error with a probability distribution of mean zero. Predictions from the deterministic simulator are made by evaluating the measured input, written as

$$\hat{\mathbf{Y}}_i^{\mathrm{o}} = \hat{f}^{\mathrm{o}}(\mathbf{X}_i), \tag{3}$$

and is referred to as the *default predictions*. The default predictions are stochastic as the measurement error in input variables is stochastic. The uncertainty brought to $\hat{\mathbf{Y}}_i^{\mathrm{o}}$ is generally analytically intractable but can be simulated. In fact, we produce independent and identically distributed Monte Carlo samples $j = 1, 2, \ldots, m$. Let $\boldsymbol{\varepsilon}_{ij}^{\mathbf{x}}$ denote input measurement errors sampled from the distribution inferred for $\boldsymbol{\varepsilon}_i^{\mathbf{x}}$. Furthermore, the model uncertainty is described by evaluating the probabilistic simulator which gives predictions $\hat{f}(\mathbf{X}_i + \boldsymbol{\varepsilon}_{ij}^{\mathbf{x}}; \boldsymbol{\theta})$. In the next sections, predictions are compared to measurements. For that comparison it is appropriate to also include sampled uncertainty in output measurements denoted $\boldsymbol{\varepsilon}_{ij}^{\mathbf{Y}}$. For convenience, this uncertainty is incorporated in the *sampled predictions* which becomes

$$\hat{\mathbf{Y}}_{ij}^{\mathrm{s}} = \hat{f}(\mathbf{X}_i + \boldsymbol{\varepsilon}_{ij}^{\mathbf{x}}; \boldsymbol{\theta}) + \boldsymbol{\varepsilon}_{ij}^{\mathbf{Y}}, \tag{4}$$

Here $\mathbf{X}_i + \boldsymbol{\varepsilon}_{ij}^{\mathbf{x}}$ simulates uncertain input and $\boldsymbol{\theta}$ are the parameters that describes the uncertainty in closure laws. Even though $\boldsymbol{\theta}$ does not have direct physical analogies, it can be estimated through its impact on $\hat{\mathbf{Y}}_{ij}^{\mathrm{s}}$. The approach is to determine $\boldsymbol{\theta}$ such that $\hat{\mathbf{Y}}_{ij}^{\mathrm{s}}$ compares to the measured output $\mathbf{Y}$.

2.3 Methods for parameter estimation

Using the framework outlined thus far, we will in this section propose two methods for estimating θ. We define two scores, being the integrated quadratic distance (IQ) and the energy score (ES). The general method is the same; for each candidate θ, sample from the corresponding model using Monte Carlo and calculate the score. Finally, the estimate of θ is

$$\hat{\theta} = \arg\min_{\theta} \text{score}(\theta), \tag{5}$$

or in the other words the parameters that minimize IQ or ES. The desired result is a simulator $\hat{f}(\mathbf{X};\theta)$ that gives accurate predictions while expressing relevant sources of uncertainty. It is clear that $\hat{f}(\mathbf{X};\theta)$ is good if it approximates the true physical value of output $f(\mathbf{x})$.

The parameters θ may be hard or computationally expensive to identify and it is useful to exclude the inconsequential parameters before commencing. If the predictions are not sensitive to closure law $\hat{g}_k$, it may be acceptable to set $G_k = \hat{g}_k$. This reduces the number of parameters and without consequential change in the predictions. Thus, it is desirable to identify the most influential closure laws as a first step of parameter estimation.

2.3.1 Integrated quadratic distance (IQ)

The difference between the default predictions and the measured output is

$$\hat{\mathbf{Y}}_i^{\text{o}} - \mathbf{Y}_i = \hat{f}^{\text{o}}(\mathbf{x}_i + \boldsymbol{\varepsilon}_i^{\mathbf{X}}) - f(\mathbf{x}_i) - \boldsymbol{\varepsilon}_i^{\mathbf{Y}}, \tag{6}$$

which is stochastic due to the measurement errors $\boldsymbol{\varepsilon}_i^{\mathbf{X}}$ and $\boldsymbol{\varepsilon}_i^{\mathbf{Y}}$. This is an observed dispersion from the true model output due to model error in the deterministic simulator and measurement error. A related quantity is the difference between the sampled predictions and the default predictions, written as

$$\hat{\mathbf{Y}}_{ij}^{\text{s}} - \hat{\mathbf{Y}}_i^{\text{o}} = \hat{f}(\mathbf{X}_i + \boldsymbol{\varepsilon}_{ij}^{\mathbf{X}};\theta) - \hat{f}^{\text{o}}(\mathbf{X}_i) + \boldsymbol{\varepsilon}_{ij}^{\mathbf{Y}}. \tag{7}$$

The sampled predictions emulates dispersion due to model error and measurement error. The terms in (7) approximates those of (6) in distribution. The distributions of measurement errors are assumed known such that the approximations $\boldsymbol{\varepsilon}_{ij}^{\mathbf{X}}$ and $\boldsymbol{\varepsilon}_{ij}^{\mathbf{Y}}$ are accurate. The sign of $\boldsymbol{\varepsilon}_{ij}^{\mathbf{Y}}$ is opposite that of $\boldsymbol{\varepsilon}_i^{\mathbf{Y}}$, but symmetry about zero is expected. Moreover, the measurement errors $\boldsymbol{\varepsilon}_i^{\mathbf{X}}$ are small such that $\mathbf{X}_i$ approximates $\mathbf{x}_i$. Similarly, the model errors are small such that $\hat{g}_k$ approximates g_k.

In summary, (7) approximates (6) when the parameters θ are appropriate. Expressions (6) and (7) will be compared across all experiments, but weights $\mathbf{W}_i$ are given to each. The weights are diagonal matrices of dimension r. Henceforth, observed errors and sampled errors refer to

$$\boldsymbol{\Delta}_i = \ (\Delta_{i1}, \Delta_{i2}, \ldots, \Delta_{ir}) \ = \mathbf{W}_i \left(\hat{\mathbf{Y}}_i^{\text{o}} - \mathbf{Y}_i \right) \tag{8a}$$

and

$$\boldsymbol{\Delta}_{ij}^{\text{s}} = (\Delta_{ij1}^{\text{s}}, \Delta_{ij2}^{\text{s}}, \ldots, \Delta_{ijr}^{\text{s}}) = \mathbf{W}_i \left(\hat{\mathbf{Y}}_{ij}^{\text{s}} - \hat{\mathbf{Y}}_i^{\text{o}} \right). \tag{8b}$$

In the case study presented below, $\mathbf{W}_i = \text{diag}\big(\hat{\mathbf{Y}}_i^{\text{o}}\big)^{-1}$ was applied such that errors are relative. Furthermore,

$$\hat{F}(\boldsymbol{\delta}) = \tfrac{1}{n} \sum_{i=1}^{n} I(\Delta_{i1} \leqslant \delta_1) I(\Delta_{i2} \leqslant \delta_2) \cdots I(\Delta_{ir} \leqslant \delta_r) \tag{9a}$$

and

$$\hat{F}^{\text{s}}(\boldsymbol{\delta};\theta) = \tfrac{1}{nm} \sum_{i=1}^{n} \sum_{j=1}^{m} I(\Delta_{ij1}^{\text{s}} \leqslant \delta_1) I(\Delta_{ij2}^{\text{s}} \leqslant \delta_2) \cdots I(\Delta_{ijr}^{\text{s}} \leqslant \delta_r) \tag{9b}$$

are empirical cumulative probability distributions and I is the indicator function. If measurement errors of different experiments are independent, the observed errors are independent but not identically distributed in general. The same applies to the sampled errors. Still, the distribution of $\boldsymbol{\Delta}_{ij}^{\mathrm{s}}$ is similar to $\boldsymbol{\Delta}_i$. The independence between experiments further implies $\hat{F}^{\mathrm{s}}$ is similar to $\hat{F}$. The distance between these distributions can be measured by the *integrated quadratic distance* which is

$$\mathrm{IQ}(\boldsymbol{\theta}) = \int_{\mathbb{R}^r} \left(\hat{F}(\boldsymbol{\delta}) - \hat{F}^{\mathrm{s}}(\boldsymbol{\delta}; \boldsymbol{\theta})\right)^2 \mathrm{d}^r\boldsymbol{\delta}, \tag{10}$$

where $\mathbb{R}^r$ is the r-dimensional real coordinate space and $\mathrm{d}^r\boldsymbol{\delta}$ is the r-dimensional volume differential. This objective function is a *proper divergence* and $\hat{F}^{\mathrm{s}}$ is close to $\hat{F}$ when IQ is small [26].

An example comparison of $\hat{F}$ and $\hat{F}^{\mathrm{s}}$ is given in Figure 1. There is one output named *pressure drop*. For now, let us look only on the black solid curve which is $\hat{F}$ and the blue dashed curve which is $\hat{F}^{\mathrm{s}}$. The IQ is the integral of the squared distance between these curves.

2.3.2 Energy score (ES)

The energy score measures how far the measured output is from the sampled predictions compared to the distance between sampled predictions themselves [27]. The energy score is separate for each experiment and is defined as

$$\mathrm{es}_i(\boldsymbol{\theta}) = \mathrm{E}\left|\left|\hat{\mathbf{Y}}_{ij}^{\mathrm{s}} - \mathbf{Y}_i\right|\right|_1 - \tfrac{1}{2}\mathrm{E}\left|\left|\hat{\mathbf{Y}}_{ij}^{\mathrm{s}} - \hat{\mathbf{Y}}_{il}^{\mathrm{s}}\right|\right|_1 \tag{11a}$$

$$\approx \tfrac{1}{m}\sum_{j=1}^{m}\left|\left|\hat{\mathbf{Y}}_{ij}^{\mathrm{s}} - \mathbf{Y}_i\right|\right|_1 - \tfrac{1}{2m^2}\sum_{j=1}^{m}\sum_{k=1}^{m}\left|\left|\hat{\mathbf{Y}}_{ij}^{\mathrm{s}} - \hat{\mathbf{Y}}_{il}^{\mathrm{s}}\right|\right|_1, \tag{11b}$$

where $\hat{\mathbf{Y}}_{ij}^{\mathrm{s}}$ and $\hat{\mathbf{Y}}_{il}^{\mathrm{s}}$ are distinct samples from the simulator and $\mathrm{E}||\cdot||_1$ is the expected value of the ℓ_1 norm. For deterministic predictions, the energy score simplifies to the absolute prediction error. It is called the *continuous ranked probability score* for univariate output. The average energy score over n experiments is

$$\mathrm{ES}(\boldsymbol{\theta}) = \tfrac{1}{n}\sum_{i=1}^{n}\mathrm{es}_i(\boldsymbol{\theta}). \tag{12}$$

The optimal value of $\boldsymbol{\theta}$ minimizes $\mathrm{ES}(\boldsymbol{\theta})$. The energy score is *strictly proper* [28] in the sense that its expected value for observed output has a unique minimum where the predictive distribution matches the observed output distribution. When the output is multivariate, each component is standardized by the mean and standard deviation across experiments in order to balance its influence [29].

3. CASE STUDIES

3.1 Simulator

Two case studies are presented, both steady-state two-phase flow in near-horizontal pipes. *Slug flow* is illustrated in Figure 2, with liquid in blue and gas as transparent. The flow direction is to the right. Liquid covers the entire bottom layer. The upper layer comprises pockets of gas separated by liquid slugs and moves with velocity U_{b} computed by an empirical closure law. Gas is also entrained as bubbles in the slugs. The slug zone holdup H_{s} is the volume fraction of liquid in the slugs. The steady-state model of choice is a momentum balance, where the main components are gravity and shear stresses. Shear stress is proportional to a dimensionless friction factor that is separate for each type of surface. The friction factor is f_{g} for the shear stress between the wall and the gas, while the liquid-wall friction factor is f_{l}. The last factor f_{i} applies to the interface between liquid and gas. In summary, the five closure laws listed Table 1 are relevant. The unit of the slug bubble velocity is meter per second and the other laws are dimensionless. All closure laws are restricted to be non-negative. Additionally the slug zone holdup cannot be greater than 1. *Stratified*

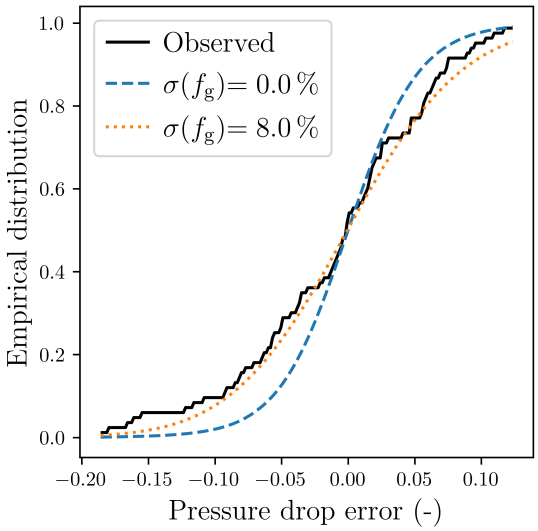

FIG. 1: Empirical distribution of the observed pressure drop error (black) and the sampled error with no model uncertainty (blue dashed) and with $\sigma(f_g) = 8.0\,\%$ (orange dotted).

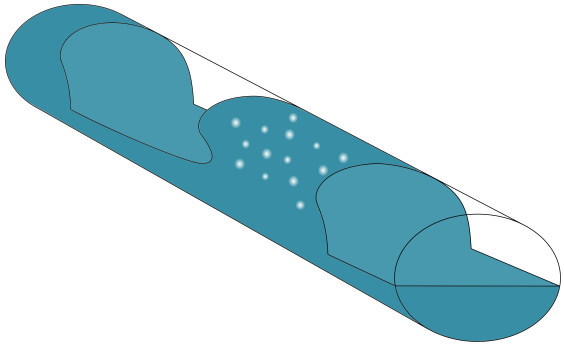

FIG. 2: Slug flow. Liquid slugs separate gas pockets. Small gas bubbles are also entrained in the slugs.

flow is essentially slug flow without the liquid slugs. *Annular flow* is characterized by a liquid film on the pipe wall and gas flowing in the center.

The physical model is implemented in the commercial multiphase simulator LedaFlow [30]. The simulator is for the purpose treated as a black box where we do not see or access the interior. It allows by default scaling of the closure law outputs by different factors. Further information about the formulation of closure laws is restricted intellectual property. A comparable flow model with all details disclosed is presented in Smith et al. [31].

3.2 Variables and measurement uncertainty

The output variables from the model are liquid holdup and the pressure drop along the pipe, where holdup is synonymous to volume fraction. The input to the model is pipe diameter, mass rates, densities, viscosities, surface tension and pipe inclination. Additionally, we have the measured pressure drop in gas-only experiments in the same pipe as an input because it is required for computing the hydraulic wall roughness. Furthermore, the *superficial velocities* U_{sg} (gas) and U_{sl} (liquid) are latent variables of great importance for the characteristics of the flow. For each phase, superficial velocity is defined as mass rate divided by density and cross-sectional area.

We label one case study as gas-dominated and the other as liquid-dominated according to superficial velocities. In Figure 3 superficial velocities are plotted for gas-dominated experiments (crosses) and liquid-dominated experiments (circles). The case studies also differ in instrumentation and consequently in standard deviations in the measurements of the pipe diameter, liquid mass rate and densities. All variables are given in table 2, with units. The third column gives the measurement standard deviation in gas-dominated flow and the last column gives the same number for liquid-dominated flow. Gaussian distributions are assumed for all measurement errors.

3.3 Closure law assumptions

Assumptions specific to the case studies are made in order to incorporate relevant knowledge and arrive at estimates for closure law uncertainties. The presented methods do not depend on these assumptions.

Probability model. Gaussian unbiased relative error $G_k(u, \mathbf{x}, \sigma_k) = \hat{g}_k(u, \mathbf{x}) \cdot \Gamma_k(\sigma_k)$, with $\Gamma_k \sim \mathcal{N}(1, \sigma_k^2)$. All information from experiments is used to quantify uncertainty parameters σ_k. If instead the focus is to tune the closure

TABLE 1: Closure laws in LedaFlow with symbol.

Closure law	Symbol
Slug zone holdup	H_{s}
Slug bubble velocity	U_{b}
Interface friction factor	f_{i}
Gas-wall friction factor	f_{g}
Liquid-wall friction factor	f_{l}

TABLE 2: Model variables with uncertainty. The first column gives the variable names of which the first two are output. The second column gives the unit. Columns three and four contain the standard deviation used in the measurement uncertainty models for the gas- and liquid-dominated experiments respectively, where x denotes the measured value, i.e. when relative error is used.

Output	Unit	Standard deviation (σ)	
		Gas-dominated	Liquid-dominated
Liquid holdup	$-$	0.01	0.01
Pressure drop	$\mathrm{Pa/m}$	$\max\left(6\,\frac{\mathrm{Pa}}{\mathrm{m}},\, x\cdot 0.01\right)$	$\max\left(6\,\frac{\mathrm{Pa}}{\mathrm{m}},\, x\cdot 0.01\right)$
Input			
Pipe diameter	m	$3.5\cdot 10^{-4}\,\mathrm{m}$	$5\cdot 10^{-4}\,\mathrm{m}$
Gas mass rate	$\mathrm{kg/s}$	$x\cdot 0.015$	$x\cdot 0.015$
Liquid mass rate	$\mathrm{kg/s}$	$x\cdot 0.02$	$x\cdot 0.003$
Gas density	$\mathrm{kg/m^3}$	$0.5\,\mathrm{kg/m^3}$	$0.1\,\mathrm{kg/m^3}$
Liquid density	$\mathrm{kg/m^3}$	$2\,\mathrm{kg/m^3}$	$1\,\mathrm{kg/m^3}$
Gas viscosity	$\mathrm{Pa\,s}$	$x\cdot 0.07$	$x\cdot 0.07$
Liquid viscosity	$\mathrm{Pa\,s}$	$x\cdot 0.02$	$x\cdot 0.02$
Surface tension	$\mathrm{N/m}$	$x\cdot 0.1$	$x\cdot 0.1$
Pipe inclination	deg	$5\cdot 10^{-3}\,\mathrm{deg}$	$5\cdot 10^{-3}\,\mathrm{deg}$
Gas-only pr. drop	$\mathrm{Pa/m}$	$x\cdot 0.01$	$x\cdot 0.01$

TABLE 3: Fluid system. Physical properties at 20 °C. The liquid-dominated experiments are all at 45 bara system pressure, while the gas-dominated experiments are either at 8, 45 or 90 bara.

Fluid	Viscosity $\left[\mathrm{Pa\,s}\right]$	Pressure $\left[\mathrm{bara}\right]$	Density $\left[\mathrm{kg/m^3}\right]$
SF_6	$1.50\cdot 10^{-5}$	8	52
Nitrogen	$1.83\cdot 10^{-5}$	45	52
		90	102
Exxsol D60	$1.55\cdot 10^{-3}$	8	815
		45	795
		90	795
Tap water	$1.00\cdot 10^{-3}$	8	1000
		45	1000
		90	1000

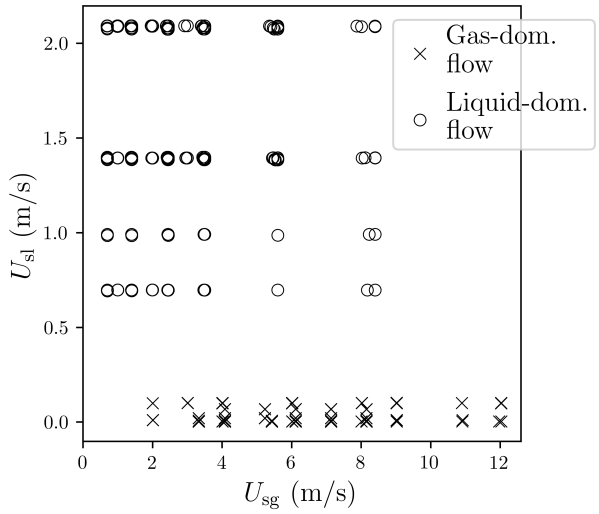

FIG. 3: Superficial velocities of the experiments for the gas-dominated study (crosses) and the liquid-dominated study (circles).

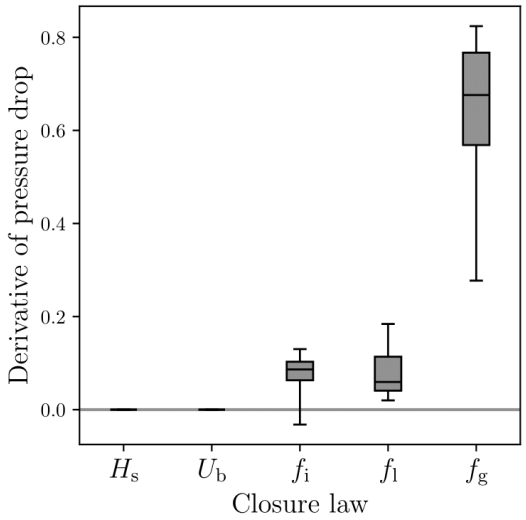

FIG. 4: Numerical derivative of pressure drop with respect to each closure law. The value is computed as a relative change with unit equal to the reciprocal of the closure law unit. Distribution over 83 experiments by percentiles 5, 25, 50, 75 and 95.

laws, one option is to define flexible errors $\Gamma_k(\mathbf{x}, \boldsymbol{\theta})$.

Independence. The closure laws may depend on each other, but errors Γ_k are assumed independent across closure laws and experiments.

Universal. Each closure laws is interpolated smoothly between a laminar and a turbulent expression. The interpolated expression is the subject of the uncertainty analysis

Numerical derivative. Numerical derivatives are used to reduce the number of parameters $\boldsymbol{\theta}$ to optimize. The relative change in output is computed for a small change in each closure law. The computation is repeated for all experiments and the closure laws with negligible influence overall are modeled as $G_k = \hat{g}_k$. The procedure may be adjusted if the relative errors in the closure laws differ in orders of magnitude.

Fluid surfaces. The error estimate assigned to each friction factor may be understood as the error in the product of the friction factor and the associated area.

3.4 Results for gas-dominated flow

This analysis regards a total of 83 gas-dominated experiments from two sites with different nominal pipe diameters. These are 4 inches (101.5 mm) in the Well Flow Loop at IFE and 8 inches (193.85 mm) in the Large Scale Facility at the SINTEF Multiphase Flow Laboratory. The experiments performed in the two facilities were otherwise similar. The pipe inclination was 2.5° upwards in both setups. In the 8-inch experiments, nitrogen was used as the gas phase, and the tests were conducted at 45 and 90 bara system pressure. In the 4-inch experiments, SF_6 was used as the gas phase at a pressure of 8 bara. At this pressure, the density of SF_6 is the same as nitrogen at 45 bara (around 52 $\mathrm{kg/m^3}$). The liquids used were Exxsol D60 and tap water. An overview of the fluid properties is supplied in table 3. The flow in these experiments was either stratified or annular.

For this data set, the pressure drop is the quantity of interest. The derivatives of the pressure drop with respect to each closure law are given in Figure 4. The derivative is computed as a relative change in pressure drop for a small change in the closure law. Each box gives quartiles one, two and three across the 83 experiments. The whiskers are the 5$^{\text{th}}$ and 95$^{\text{th}}$ percentiles. As expected, the slug zone holdup H_{s} and the slug bubble velocity U_{b} do not affect the pressure drop as they are not used in stratified or annular flows. It is also clear that the dominating closure law

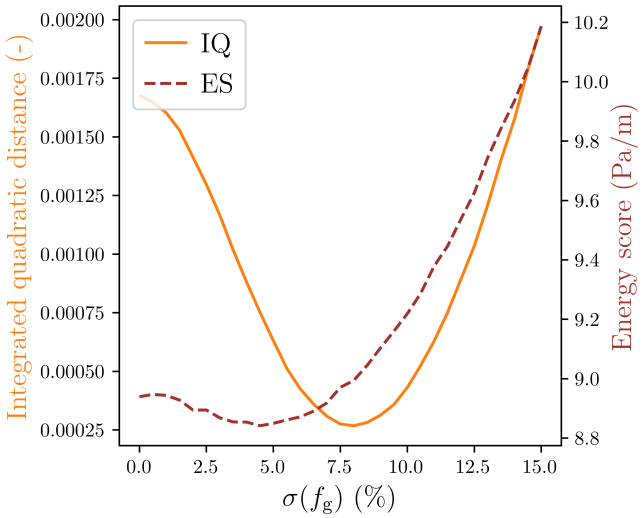

FIG. 5: Integrated quadratic distance (orange) and energy score (red dashed) with respect to uncertainty in f_g for gas-dominated experiments.

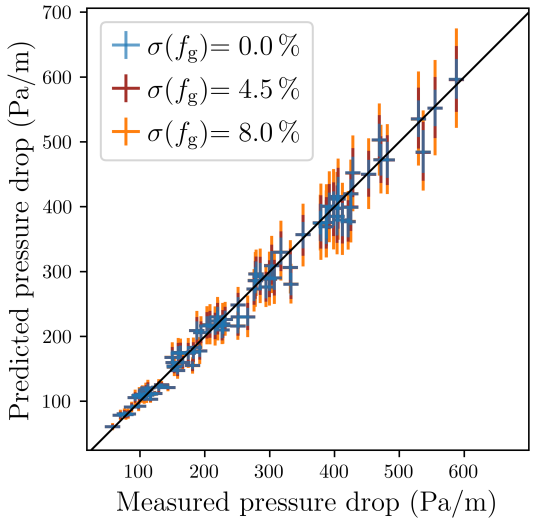

FIG. 6: Predicted versus measured pressure drop for 83 experiments with no model uncertainty (blue), with 4.5 % relative error in f_g (red) and 8.0 % (orange). The black line is where the coordinates are equal. Means and 95 % prediction intervals are given for both predictions and measurements.

for this data set is the gas-wall friction factor f_g. Thus, we estimate the uncertainty of f_g using the pressure drop measurements. The remaining closure laws are assumed known, which is $\Gamma_k = 1$.

Figure 5 shows the integrated quadratic distance (orange) and energy score (red dashed) with respect to $\sigma(f_g)$ for gas-dominated experiments, based on 10 000 Monte Carlo predictions for each. The IQ is minimal at $\sigma(f_g) = 8.0\,\%$ while ES is minimal at $\sigma(f_g) = 4.5\,\%$. The uncertainties in the four other closure laws are taken as zero. Figure 1 provides a closer look at the IQ computation. The black line is the observed error distribution for pressure drop defined in (9a). The blue dashed line is the sampled error defined in (9b) with no model uncertainty and the orange dotted line is equivalent with $\sigma(f_g) = 8.0\,\%$. This parameter value put the sampled distribution closest to the observed distribution and is consequently minimizing IQ.

The quality of the estimate for model uncertainty may be assessed with Figure 6. The predicted pressure drops are compared with the measurements. Due to their uncertainty, each prediction and measurement are distributions, and they are represented by means and 95 % prediction intervals. The interval limits are percentiles 2.5 and 97.5 of the output distributions, which for measurements are normal distributions with σ from Table 2, and for predictions are Monte Carlo samples $\{\hat{\mathbf{Y}}^{\mathrm{s}}_{ij}\}_{j=1}^{m}$.

The black diagonal line is where predictions equal measurements. The blue points describe the situation with no model uncertainty while red (ES) and orange (IQ) points are tuned by the optimal model uncertainty. For one experiment, combining the horizontal interval and vertical interval to one wider interval yields the 95 % prediction interval for a sampled prediction $\hat{\mathbf{Y}}^{\mathrm{s}}_{ij}$ from (4). The *coverage* is defined as the fraction of experiments where combined horizontal/vertical interval contains the measured pressure drop. The coverage of the deterministic simulator is 92 % and the coverage of the probabilistic simulator is 94 % for ES and 96 % for IQ.

3.5 Results for liquid-dominated flow

The liquid-dominated study includes 152 experiments conducted in the Large Scale Facility at the SINTEF Multiphase Flow Laboratory. For a detailed description we refer to a previous experimental paper [32]. The fluids ran in an 8-inch carbon steel piping with an internal diameter of 189 mm. There was one 359 m long horizontal section connected to a 366 m long section of inclination 0.5°. The system pressure was 45 bara, and nitrogen was used for

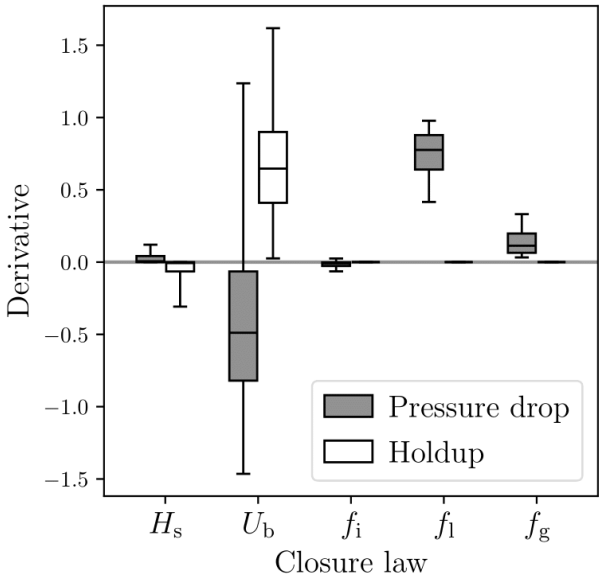

FIG. 7: Numerical derivative of pressure drop (*gray*) and holdup (*white*) with respect to each closure law. The value is computed as a relative change with unit equal to the reciprocal of the closure law unit. Distribution over 152 experiments by percentiles 5, 25, 50, 75 and 95.

the gas phase. The liquids used in the experiments were Exxsol D60 and tap water. The fluid properties are listed in table 3.

The computations for liquid-dominated flow are identical to those of gas-dominated flow. Consequently, some results are presented more briefly in this section. Firstly, the derivatives of the predictions with respect to each closure law were computed. Their distributions across the 152 experiments are drawn in Figure 7 for pressure drop (gray) and holdup (white). The closure laws for U_b and f_l have the greatest impacts. Their contributions to model uncertainty are investigated further, while the other closure laws are treated as deterministic. For each pair of $\sigma(U_\mathrm{b})$ and $\sigma(f_\mathrm{l})$ investigated, 10 000 Monte Carlo predictions are produced. Figure 8 gives the IQ (left) and ES (right) of each combination of standard deviations. The color of each square gives the score for the parameter values given on the axes. The optimal parameters are $\sigma(U_\mathrm{b}) = 3.5\,\%$ and $\sigma(f_\mathrm{l}) = 4.5\,\%$ for IQ and $\sigma(U_\mathrm{b}) = 4.0\,\%$ and $\sigma(f_\mathrm{l}) = 5.5\,\%$ for ES.

Figure 9 shows the joint empirical distributions for pressure drop error and holdup error. The observed error (gray) is compared with the sampled error from the deterministic simulator (blue) and the IQ probabilistic simulator (orange). For each plot, the IQ is the squared integrated distance between the two surfaces. These IQ-values are found in the left panel of Figure 8. A comparison of predictions and measurements are given in Figure 10 for pressure drop (left) and holdup (right) for the deterministic simulator (blue), the probabilistic simulator with IQ-parameters (orange) and the probabilistic simulator with ES-parameters (red). The coverage for the deterministic simulator is 86 % for pressure drop and 88 % for holdup. The coverages with IQ-parameters are 100 % for pressure drop and 96 % for holdup, while the coverages with ES-parameters are 100 % for pressure drop and 97 % for holdup.

The slug bubble velocity U_b was measured directly for these experiments, which serves as validation of the method presented. Figure 11 gives the error distribution for U_b using the direct measurements. The distribution has a mean of $\mu(U_\mathrm{b}) = 96.4\,\%$ and a standard deviation of $\sigma(U_\mathrm{b}) = 3.5\,\%$. The standard deviation assuming $\mu(U_\mathrm{b}) = 1$ is $\sigma(U_\mathrm{b}) = 5.0\,\%$.

4. DISCUSSION

Closure law uncertainties are integral to a probabilistic simulator. Two accessible methods for estimating uncertainty in closure laws have been demonstrated on the commercial multiphase flow simulator LedaFlow. By evaluating a

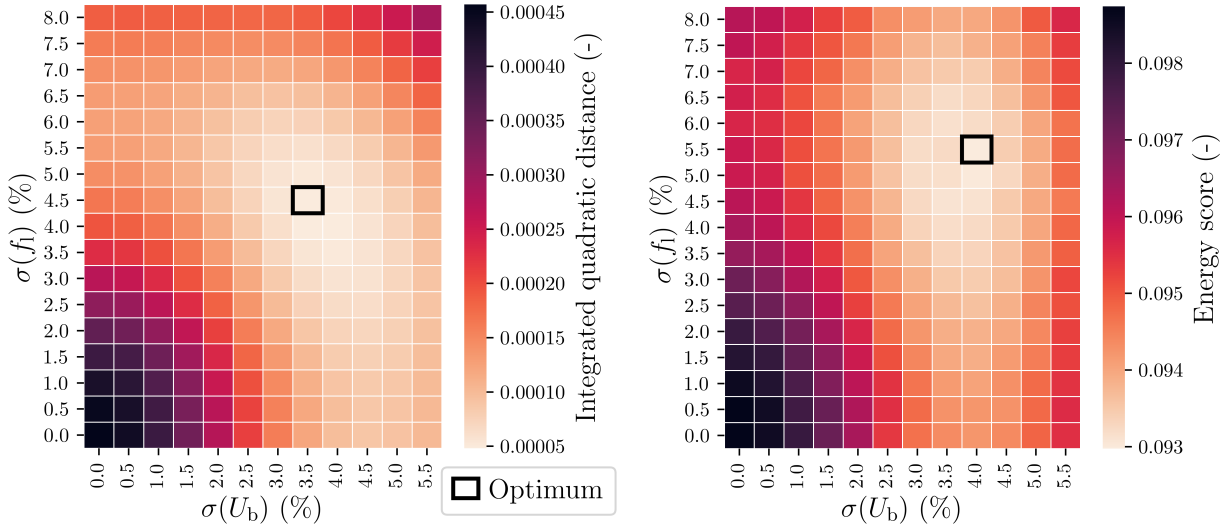

FIG. 8: Integrated quadratic distance (left) and energy score (right) for combinations of $\sigma(U_\mathrm{b})$ and $\sigma(f_\mathrm{l})$. The optimal scores are highlighted.

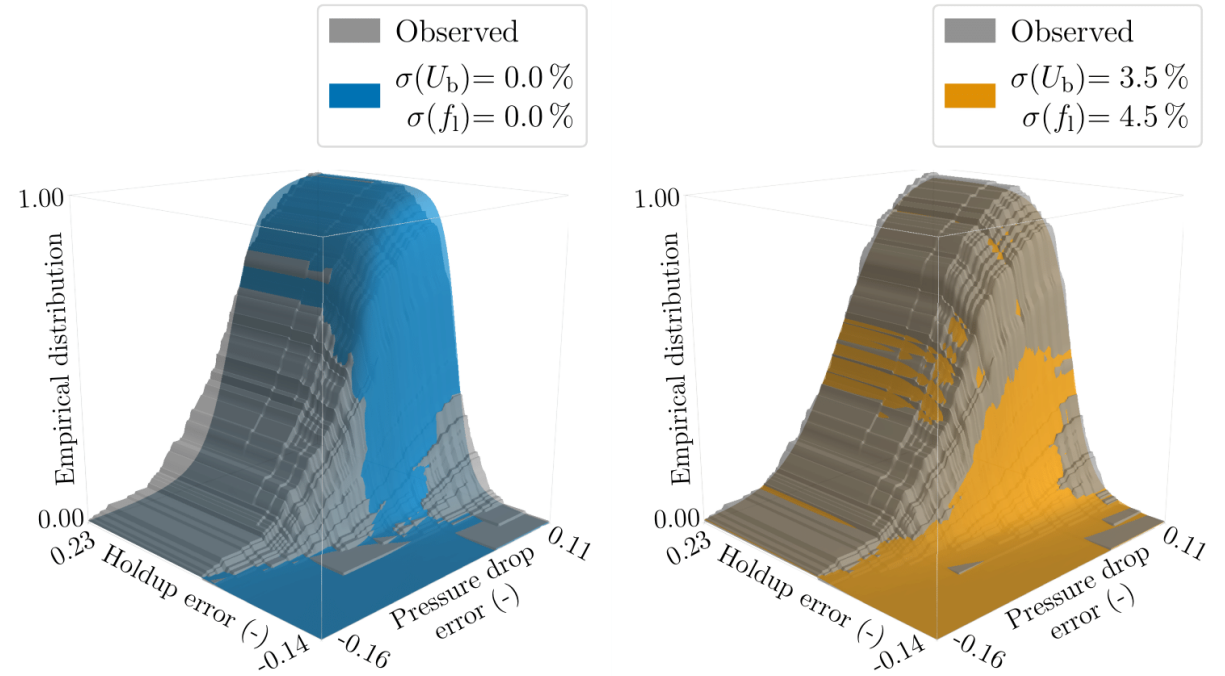

FIG. 9: Empirical distribution of the observed pressure drop and holdup error (gray) and the sampled error with no model uncertainty (blue) and with $\sigma(U_\mathrm{b}) = 3.5\,\%$ and $\sigma(f_\mathrm{l}) = 4.5\,\%$ (orange).

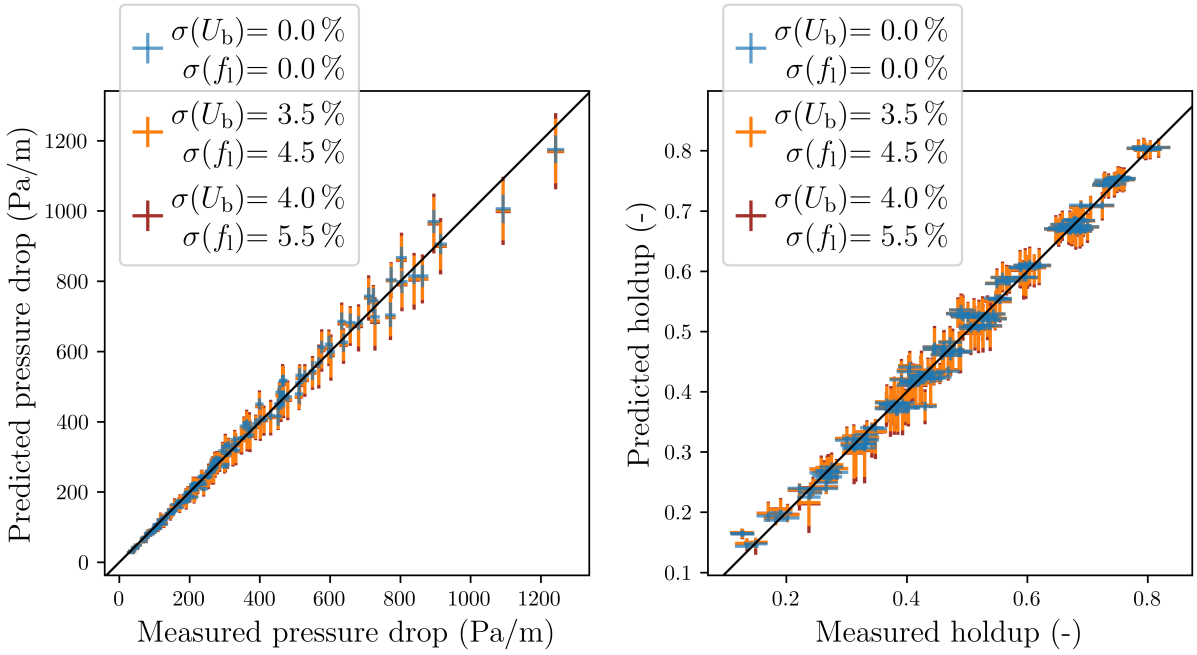

FIG. 10: Predicted versus measured pressure drop (left) and holdup (right) for 152 experiments for the deterministic simulator (blue), the probabilistic simulator with IQ-parameters (orange) and the probabilistic simulator with ES-parameters (red). The black line is where the coordinates are equal. Means and 95 % prediction intervals are given for both predictions and measurements.

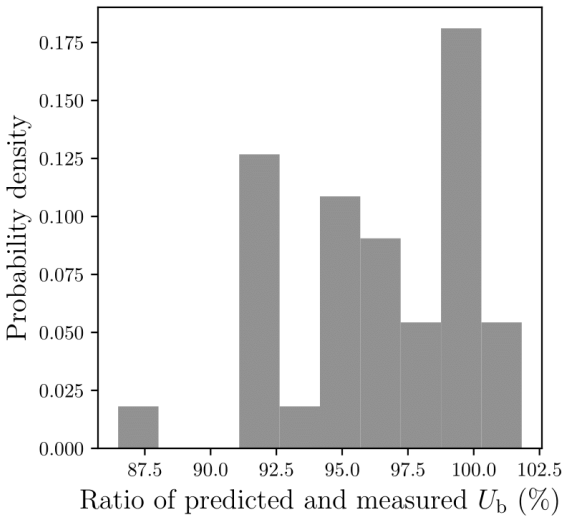

FIG. 11: The predicted values of U_b divided by the direct measurements. The mean is $\mu(U_b) = 96.4\,\%$ and standard deviation is $\sigma(U_b) = 3.5\,\%$.

probabilistic simulator at input with sampled measurement error, we achieved predictions that incorporated both model uncertainty and measurement uncertainty in input and output variables. The closure law standard deviation was estimated using data from two recent experimental campaigns.

The integrated quadratic distance were used to match the distribution of sampled errors to the distribution of observed errors across experiments. The energy score was computed separately for each experiment and is a measure for the distance between the sampled predictions and the measured output. The IQ and ES behaved differently with respect to θ in some manners. In fact, predictive distributions were sharper for the ES. However, there is a general trade-off between sharpness and calibration. Two objective functions were investigated in this study because both are intuitive and proper, which demonstrates the subjective aspect of probabilistic predictions. Thus, it is necessary to tailor the objective function to the application.

Optimal parameters by IQ correspond to sampled error distributions close to the observed error distributions, in the sense of minimizing (10). The predictions with optimal parameter values were plotted against measurements to demonstrate the clear improvement in predictions when the model uncertainty was included. The improvement was seen both visually and in terms of coverage, for both IQ and ES. The coverages were similar for IQ and ES and generally higher than the expected 95 $\%$.

We made a number of assumptions to achieve a statistical framework. The model uncertainty was attributed to the closure laws entirely as the major approximations in the simulator are the closure laws. The closure law assumptions specific to the case studies are listed in Section 3.3. The assumptions would be relaxed if proven inapt. The error was modeled as relative to the closure law value, with the same distribution across all experiments. The framework is not restricted to identically distributed relative errors. In fact, applications with different prior knowledge of the errors can implement this knowledge into the assumed distributions, for instance by adding a bias to be tuned along with the standard deviation [33]. An example of bias estimation is given in the appendix, but it is not evident that bias is necessary for our case studies. LedaFlow is already expected to be carefully tuned from large amounts of data, and uncertainty quantification seems more pressing than tuning.

The derivative of the outputs with respect to each closure law informed the optimization procedure in our application. However, this procedure can fail if the realistic ranges of the closure laws are of different orders of magnitude. Other preliminary analyses may then be considered. Trial and error for optimizing parameter values is acceptable because we can check the closeness of the error distributions or the prediction coverage afterwards. The preliminary analysis indicated that the observed error in holdup for the gas-dominated experiments could be explained by measurement uncertainty alone. Data with large measurement uncertainty compared to observed error naturally give limited information about model uncertainty.

The methods are directly applicable to any number of closure laws, inputs and outputs. There may be practical limitations such as computational cost. The parameter optimization applied was plainly to compute IQ or ES for a series of plausible parameter values and chose the parameters of the optimum. This task grows combinatorially with the number of closure laws involved. If the simulator is computationally expensive or many closure laws are influential, it may still be feasible to find an optimum with an iterative algorithm.

Ultimately, it matters how the methods perform for a real industrial process. The performance depends strictly on what data is available. The optimal scenario is to have field data, and the second best scenario is to have laboratory data that matches the most important dimensionless numbers of field [34]. In either case, the methods described in Section 2 can be applied directly to obtain realistic prediction intervals incorporating measurement and model uncertainty. Experimental validation of uncertainty estimates for full scale is still useful, but not yet available. In contrast, if the data available does not match the dimensionless numbers of the field process, the uncertainty analysis will not be representative.

Oliver et al. [25] studied a mass-spring-damper system, where closure law uncertainty estimates were supported by qualitative information about model misspecification. They considered a scalar damping coefficient with an unknown dependency on temperature. However, dimensional analysis proved that the rate of temperature change was inversely proportional to mass. Consequently, the estimated uncertainty about the damping coefficient was conservative when extrapolated to systems with larger masses. In summary, additional insight into model misspecification may allow for extrapolation of uncertainty estimates. Extrapolation is a useful extension of the methods presented in this paper or elsewhere.

5. CONCLUSIONS

We have presented new methods to quantify uncertainty in the closure laws of a simulator. The methods are useful for commercial simulators where the formulation of the closure laws are not disclosed in order to protect intellectual property rights. The simulator is still required to have tuning capabilities such that the simulator output with respect to the most important closure laws can be gauged. The purpose of estimating closure law uncertainties is to provide predictions of real applications with realistic uncertainty estimates. For instance, in petroleum production systems, where a quantified model uncertainty is strictly necessary for a robust design.

Monte Carlo simulations were used to propagate the uncertainties in regular input variables, which were known, along with candidate values for uncertainty in the closure laws. Different parameter values yielded different distributions of predictions, and we selected the parameter values that gave the best agreement with measurements.

The methods were applied to the commercial multiphase simulator LedaFlow on two fundamentally different data sets. The first comprises 83 gas-dominated experiments and the other 152 liquid-dominated experiments. For the gas-dominated experiments describing model uncertainty by $\sigma(f_{\mathrm{g}}) = 8.0\,\%$ optimizes IQ. The energy score is in this case more conservative and yields $\sigma(f_{\mathrm{g}}) = 4.5\,\%$ The model uncertainty in the liquid-dominated experiments is $\sigma(U_{\mathrm{b}}) = 3.5\,\%$ and $\sigma(f_{\mathrm{l}}) = 4.5\,\%$ for IQ, and $\sigma(U_{\mathrm{b}}) = 4.0\,\%$ and $\sigma(f_{\mathrm{l}}) = 5.5\,\%$ for ES. The estimate of $\sigma(U_{\mathrm{b}})$ is admissible by validation with direct measurements of U_{b}.

We have demonstrated estimation of model uncertainty from laboratory experiments. The resulting probabilistic simulator can be deployed in real processes with similar flow conditions. In general we recommend the following steps for the design and work flow of an industrial process.

1. Build a model of the system using an appropriate simulation framework.

2. Establish the most important input variables and assess their individual ranges and uncertainties for the lifetime of the process.

3. Find laboratory data that matches the relevant dimensionless numbers of the process, and apply the proposed method to quantify the uncertainties in the most important closure laws.

4. Apply the estimated uncertainties in the closure law and the known uncertainties in the input variables through Monte Carlo simulations of the real process to establish realistic probability distributions of the critical model output.

5. Revise the system design as necessary based on the simulations in line with the organization's risk management guidelines such as compliance with the required confidence level.

ACKNOWLEDGMENTS

This work is part of the project SUM (Scaling and Uncertainty in Multiphase Flow), which is supported by the Norwegian Research Council grant number 267620 and industrial partners from SINTEF, IFE and MULTIFLOW JIP (Schlumberger Information Solution, Equinor, ESSS, Lundin Norway, LedaFlow Technologies DA, Gassco, Vår Energi and TechnipFMC).

APPENDIX A. BIAS PARAMETERS

The analysis for the liquid-dominated experiments is repeated with additional parameters included. We allow for a bias in both U_{b} and f_{l}. The original value for U_{b} in LedaFlow is multiplied by normally distributed variable with mean $\mu(U_{\mathrm{b}})$ and standard deviation $\sigma(U_{\mathrm{b}})$, and f_{l} is treated alike. The IQ values for 1000 Monte Carlo samples of selected parameter values are given in Figure A.12. Each panel in the 4×4 grid corresponds to a value for $\sigma(f_{\mathrm{l}})$ (top) and $\sigma(U_{\mathrm{b}})$ (right). Within each panel, the values of $\mu(U_{\mathrm{b}})$ (left) and $\mu(f_{\mathrm{l}})$ (bottom) ranges from $96\,\%$ to $104\,\%$ of the flow model value. An unbiased model corresponds to $\mu = 100\,\%$ which is realistic for this application.

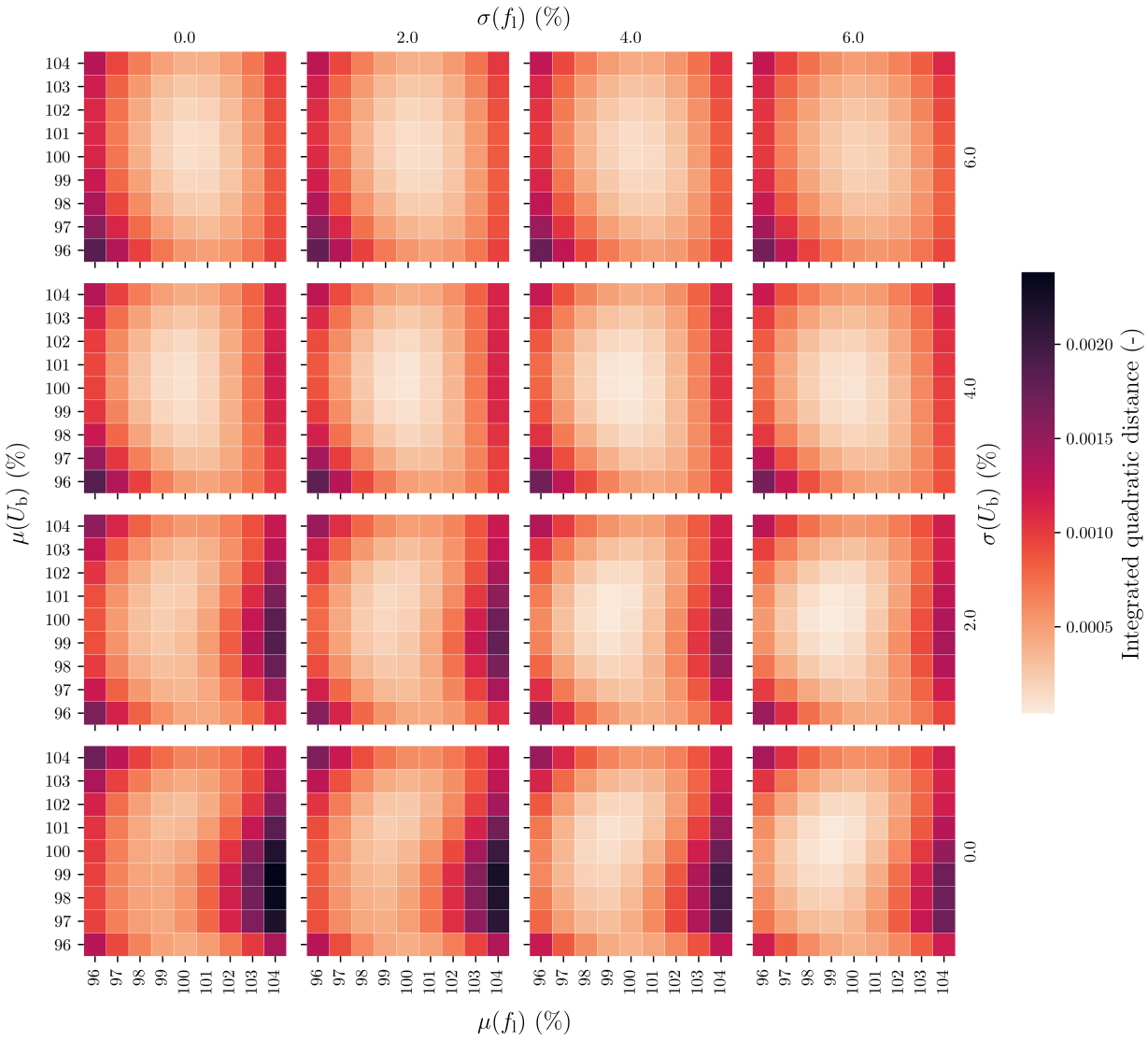

FIG. A.12: Integrated quadratic distance for 152 liquid-dominated experiments in terms of four uncertainty parameters. Bias in U_b (left), bias in f_1 (bottom), standard deviation in U_b (right) and standard deviation in f_1 (top). The top and right coordinates refers to a panel in the 4×4 grid.

REFERENCES

1. Ohm, G.S., *The Galvanic circuit investigated mathematically*, D. Van Nostrand Company, New York, 1905.
2. Drude, P., Zur elektronentheorie der metalle, *Annalen der physik*, 306(3):566–613, 1900.
3. Clapeyron, É., Mémoire sur la puissance motrice de la chaleur, *Journal de l'École polytechnique*, 14:153–190, 1834.
4. Darcy, H., *Les fontaines publiques de la ville de Dijon: exposition et application...*, Victor Dalmont, 1856.
5. Bejan, A., *Convection heat transfer*, John wiley & sons, 2013.
6. Brennen, C.E. and Brennen, C.E., *Fundamentals of multiphase flow*, Cambridge university press, 2005.
7. Boyack, B., Catton (UCLA), I., Duffey (INEL), R., Griffith (MIT), P., Katsma (INEL), K., Lellouche, G., Levy (S. Levy Inc.), S., Rohatgi (BNL), U., Wilson (INEL), G., Wulff (BNL), W., and Zuber (USNRC), N., Quantifying reactor safety margins part 1: An overview of the code scaling, applicability, and uncertainty evaluation methodology, *Nuclear Engineering and Design*, 119(1):1–15, 1990.
8. Wilson, G.E., Boyack, B., Catton, I., Duffey, R., Katsma, K., SLI, G.L., SLI, S.L., and NRC, N.Z., Quantifying reactor safety margins part 2: Characterization of important contributors to uncertainty, *Nuclear Engineering and Design*, 119(1):17–31, 1990.
9. Wulff, W., Boyack, B., Catton, I., Duffey, R., Katsma, K., SLI, G.L., SLI, S.L., Wilson, G., and USNRC, N.Z., Quantifying reactor safety margins part 3: Assessment and ranging of parameters, *Nuclear Engineering and Design*, 119(1):33–65, 1990.
10. Lellouche, G., Levy, S., Boyack (LANL), B., Catton (UCLA), I., Duffy (INEL), R., Griffith, P., Katsma (INEL), K., MAY (SLI), R., Rohatgi (BNL), U., Wilson (INEL), G., Wulff (BNL), W., and Zuber (NRC), N., Quantifying reactor safety margins part 4: Uncertainty evaluation of lbloca analysis based on trac-pf1/mod 1, *Nuclear Engineering and Design*, 119(1):67–95, 1990.
11. Zuber, N., Wilson, G.E., Boyack (LANL), B.E., Catton (UCLA), I., Duffey (INEL), R.B., Griffith (MIT), P., Katsma (INEL), K.R., Lellouche (SLI), G.S., Levy (SLI), S., Rohatgi (BNL), U.S., and Wulff (BNL), W., Quantifying reactor safety margins part 5: Evaluation of scale-up capabilities of best estimate codes, *Nuclear Engineering and Design*, 119(1):97–107, 1990.
12. Catton, I., Duffey, R., Shaw, R., Boyack, B., Katsma, K., SLI, G.L., SLI, S.L., Wilson, G., and NRC, N.Z., Quantifying reactor safety margins part 6: a physically based method of estimating PWR large break loss of coolant accident pct, *Nuclear engineering and design*, 119(1):109–117, 1990.
13. Shaw, R.A., Larson, T.K., and Dimenna, R.K., Development of a phenomena identification and ranking table (PIRT) for thermal – hydraulic phenomena during a PWR LBLOCA, Tech. Rep. NUREG/CR-5074, Idaho National Engineering Lab., 1988.
14. Wulff, W., Uncertainties in modeling and scaling in the prediction of fuel stored energy and thermal response, Tech. Rep. BNL-NUREG-40498, Brookhaven National Lab., 1987.
15. Cremaschi, S., Kouba, G.E., and Subramani, H.J., Characterization of confidence in multiphase flow predictions, *Energy & fuels*, 26(7):4034–4045, 2012.
16. Picchi, D. and Poesio, P., Uncertainty quantification and global sensitivity analysis of mechanistic one-dimensional models and flow pattern transition boundaries predictions for two-phase pipe flows, *International Journal of Multiphase Flow*, 90:64–78, 2017.
17. Strand, A., Smith, I.E., Unander, T.E., Steinsland, I., and Hellevik, L.R., Uncertainty propagation through a point model for steady-state two-phase pipe flow, *Algorithms*, 13(3):53, 2020.
18. Holm, H., Saha, P., Suleymanov, V., Vanvik, T., Hoyer, N., , Shtokman flow assurance challenges–a systematic approach to analyze uncertainties–part 1, In *15th International Conference on Multiphase Production Technology*, pp. 173–189. BHR Group, 2011.
19. Holm, H., Saha, P., Suleymanov, V., Vanvik, T., Hoyer, N., , Shtokman flow assurance challenges–a systematic approach to analyze uncertainties–part 2, In *15th International Conference on Multiphase Production Technology*, pp. 191–206. BHR Group, 2011.
20. Hoyer, N., Kirkedelen, M., Biberg, D., Johnson, G., Valle, A., Johansson, P., Nossen, J., , A structured approach for the evaluation of uncertainties in flow assurance systems, In *16th International Conference on Multiphase Production Technology*, pp. 77–91. BHR Group, 2013.
21. Wang, J., Wu, J.L., and Xiao, H., Incorporating prior knowledge for quantifying and reducing model-form uncertainty in

RANS simulations, *International Journal for Uncertainty Quantification*, 6(2), 2016.

22. Xiao, H. and Cinnella, P., Quantification of model uncertainty in RANS simulations: A review, *Progress in Aerospace Sciences*, 108:1–31, 2019.
23. Beck, J.L., Bayesian system identification based on probability logic, *Structural Control and Health Monitoring*, 17(7):825–847, 2010.
24. Beck, J.L. and Taflanidis, A., Prior and posterior robust stochastic predictions for dynamical systems using probability logic, *International Journal for Uncertainty Quantification*, 3(4), 2013.
25. Oliver, T.A., Terejanu, G., Simmons, C.S., and Moser, R.D., Validating predictions of unobserved quantities, *Computer Methods in Applied Mechanics and Engineering*, 283:1310–1335, 2015.
26. Thorarinsdottir, T.L., Gneiting, T., and Gissibl, N., Using proper divergence functions to evaluate climate models, *SIAM/ASA Journal on Uncertainty Quantification*, 1(1):522–534, 2013.
27. Gneiting, T., Stanberry, L.I., Grimit, E.P., Held, L., and Johnson, N.A., Assessing probabilistic forecasts of multivariate quantities, with an application to ensemble predictions of surface winds, *Test*, 17(2):211, 2008.
28. Gneiting, T. and Raftery, A.E., Strictly proper scoring rules, prediction, and estimation, *Journal of the American statistical Association*, 102(477):359–378, 2007.
29. Möller, A., Lenkoski, A., and Thorarinsdottir, T.L., Multivariate probabilistic forecasting using ensemble bayesian model averaging and copulas, *Quarterly Journal of the Royal Meteorological Society*, 139(673):982–991, 2013.
30. Kjølaas, J., De Leebeeck, A., and Johansen, S., Simulation of hydrodynamic slug flow using the ledaflow slug capturing model, In *16th International Conference on Multiphase Production Technology*. BHR Group, 2013.
31. Smith, I.E., Nossen, J., Kjølaas, J., and Lund, B., Development of a steady-state point model for prediction of gas/oil and water/oil pipe flow, *Journal of Dispersion Science and Technology*, 36(10):1394–1406, 2015.
32. Kjølaas, J., Unander, T.E., Wolden, M., Schümann, H., Leinan, P.R., Smith, I.E., and Shmueli, A., Large scale experiments on slug length evolution in long pipes, In *OTC Offshore Technology Conference*, Vol. Day 4 Thu, May 07, 2020.
33. Paudel, D. and Hostikka, S., Propagation of modeling uncertainty in stochastic heat-transfer simulation using a chain of deterministic models, *International Journal for Uncertainty Quantification*, 9(1), 2019.
34. Farokhpoor, R., Liu, L., Langsholt, M., Hald, K., Amundsen, J., and Lawrence, C., Dimensional analysis and scaling in two-phase gas–liquid stratified pipe flow–methodology evaluation, *International Journal of Multiphase Flow*, 122:103139, 2020.